Research Article Vol. 9, No. 5 / May 2021 / Photonics Research 741

PHOTONICS Research

Single-mode spatiotemporal soliton attractor in multimode GRIN fibers

M. Zitelli,[1,*] M. Ferraro,[1] F. Mangini,[2] and S. Wabnitz[1,3]

[1]Department of Information Engineering, Electronics and Telecommunications (DIET), Sapienza University of Rome, 00184 Rome, Italy
[2]Department of Information Engineering (DII), University of Brescia, 25123 Brescia, Italy
[3]Novosibirsk State University, Novosibirsk 630090, Russia
*Corresponding author: mario.zitelli@uniroma1.it

Received 6 January 2021; revised 23 February 2021; accepted 23 February 2021; posted 23 February 2021 (Doc. ID 419235); published 26 April 2021

Experimental and numerical studies of spatiotemporal femtosecond soliton propagation over up to 1 km spans of parabolic graded-index fibers reveal that initial multimode soliton pulses naturally and irreversibly evolve into a single-mode soliton. This is carried by the fundamental mode of the fiber, which acts as a dynamical attractor of the multimode system for up to the record value (for multimode fibers) of 5600 chromatic dispersion distances. This experimental evidence invalidates the use of variational approaches, which intrinsically require that the initial multimode propagation of a self-imaging soliton is indefinitely maintained.

https://doi.org/10.1364/PRJ.419235

1. INTRODUCTION

Optical solitons in fibers have been extensively and successfully studied over the past 50 years, leading to significant progress in long-distance optical communications and mode-locked lasers [1,2]. Although nearly all of these investigations involved the generation and propagation of single-mode fiber solitons, optical solitons can be supported by multimode optical fibers (MMFs) as well [3–6].

Interest in MMFs has been motivated by their potential for increasing the transmission capacity of long-distance optical links via the technique of mode-division multiplexing (MDM), exploiting the multiple transverse modes of the fiber as information carriers [7]. In this context, it has been predicted that, in the presence of random mode coupling and nonlinearity, MMFs can support the stable propagation of Manakov solitons, leading to a nonlinear compensation of modal dispersion [8,9]. The possibility of overcoming modal dispersion is also of great interest for high-speed local area networks, where MMFs are extensively employed [10]. In addition, there is a significant industrial interest in the use of large-area fibers for up-scaling the power of fiber lasers, for high-power beam delivery, and for biomedical imaging applications. In these applications, it is very important to maintain the high beam quality of single-mode fibers even when transporting a beam via an MMF [11,12].

When compared with single-mode fiber solitons, experimental studies of optical solitons in MMFs remain relatively scarce. The analysis of the propagation of femtosecond pulses undergoing soliton self-frequency shift (SSFS) in graded-index (GRIN) MMFs has revealed that multiple transverse modes are effectively mutually trapped by cross-phase modulation, in spite of their strong linear temporal walk-off due to modal dispersion [13–17].

To date, the dynamics and stability of MMF solitons remain yet to be assessed. Theoretical treatments of spatiotemporal soliton propagation in MMFs mostly rely on the variational approach (VA) [18,19]. When neglecting the temporal dimension, the variational method permits to include the Kerr effect in the description of the periodic spatial self-imaging (SSI) which occurs in GRIN MMFs [20]. Based on this VA, and by adding group-velocity dispersion, it has been proposed that soliton propagation in MMFs can be theoretically described in terms of a reduced one-dimensional generalized nonlinear Schrödinger equation with a spatially varying effective mode area [21–23]. The validity of the VA is based on the assumption that the initial beam shape is maintained unchanged upon propagation, except for a limited set of slowly varying parameters (e.g., the beam amplitude and width).

Now, early experiments of soliton generation in GRIN MMFs have demonstrated that optical solitons generated by a highly multimode pump via the mechanism of Raman cascade and SSFS are essentially carried by the fundamental mode of the fiber [24]. Although the mechanism of spatial beam reshaping for soliton pulses remained largely unexplained, it was attributed to a process of Raman beam clean-up. In recent years, new experiments revealed that the Kerr effect can also lead to spatial beam self-cleaning in GRIN MMFs. In this case, an irreversible transfer of energy toward the fundamental mode of the fiber is induced by modal four-wave mixing (FWM) processes, quasi-phase-matched by SSI [25]. The occurrence of spatial beam self-cleaning has been investigated both in

the normal [25–27] and anomalous dispersion regimes of MMFs [28], but only in situations where temporal (chromatic and modal) dispersion does not play a role.

In this work, we theoretically and experimentally demonstrate, we believe for the first time, the spatial beam cleaning of multimode solitons in GRIN MMFs. An initially excited multimode femtosecond soliton composed by a few low-order transverse modes, irreversibly decays into a single-mode soliton, owing to the FWM-induced energy transfer of higher-order modes into the fundamental mode of the MMF. Once formed, the single-mode soliton remained stable over the tested fiber length of 1 km, which corresponds to the record transmission distance in an MMF of 4600 modal dispersion distances, and 5600 chromatic dispersion lengths. This effect is of particular importance for technological applications, as it reveals that nonlinearity can counteract the effects of modal dispersion and random mode coupling and enable the stable transport of high spatial quality beams over long distances by means of large-area MMFs. As a side aspect, our results invalidate theoretical predictions based on the VA, since the beam shape substantially evolves along the fiber, in a way that the initial beam profile is not maintained.

2. TRANSMISSIONS UP TO 1 km OF GRIN FIBER

In this section, we provide a detailed description of the spatiotemporal evolution of multimode femtosecond solitons in long spans of parabolic GRIN fibers. Experimental characterizations of the output pulse width, bandwidth, and beam shape are supported by successful comparisons with extensive numerical simulations.

A. Model and Simulations

A numerical model suitable for studying the propagation of multimodal pulses over long spans of GRIN fiber is based on the coupled-mode equations approach [29], which requires a preliminary knowledge of the input power distribution among the fiber modes. The model couples the propagating mode fields via Kerr and Raman nonlinearities, via FWM terms of the type $Q_{plmn}A_lA_mA_n^*$; the coupling coefficients Q_{plmn} are proportional to the overlap integrals of the transverse modal field distributions. We modified the standard coupled-mode generalized nonlinear Schrödinger equations of Poletti and Horak [29], as implemented by Wright *et al.* as open-source MATLAB parallel numerical mode solver [30], in order to include the wavelength-dependent linear losses of silica. Fiber dispersion and nonlinearity parameters are estimated to be $\beta_2 = -28.8$ ps^2/km at 1550 nm, $\beta_3 = 0.142$ ps^3/km, nonlinear index $n_2 = 2.7 \times 10^{-20}$ m^2/W, and Raman response $h_r(\tau)$ with typical times of 12.2 and 32 fs [31,32].

When considering a beam entering the fiber with no input tilt angle, and focused on the entry face with a 30 μm ($1/e^2$) diameter, by means of a specific software we calculated the input mode relative power distribution to be 52%, 30%, and 18% for the first three axial-symmetric modes LP_{01}, LP_{02}, and LP_{03}, respectively; other higher-order modes carry negligible power. The sums over l, m, and n of the FWM coupling coefficients Q_{1lmn}, Q_{2lmn}, and Q_{3lmn}, responsible for feeding the three modes are 4.67×10^9, 4.17×10^9, and 3.50×10^9 m^{-2}, respectively; the number of coefficients larger than the mean value is 37, out of which 16 couple to the mode LP_{01}, 11 to the LP_{02}, and 10 to the LP_{03}. The lack of symmetry between coupling coefficients is responsible for a slow, but irreversible transfer of energy from higher-order modes toward the fundamental, when pulses carried by different modes are temporally and spatially overlapping.

Figure 1 shows the simulated evolution along the GRIN fiber of the pulse energy in each of the three propagating modes (bottom left), and their corresponding center wavelength (bottom right). Here we coupled at the fiber input a Gaussian pulse with 67 fs duration, 1550 nm wavelength, 30 μm diameter (at $1/e^2$ of peak intensity), and 28 kW of peak power, which is suitable for spatiotemporal soliton generation. The top left inset shows the input temporal power profile for each of the three modes. During propagation over the first 10 m of fiber (see the wavelength panel in Fig. 1), the three modes separate their wavelengths, which permits them to experience different chromatic dispersions, which leads to a group-velocity difference that exactly compensates for modal dispersion walk-off. As a result, the three modes propagate together with the same speed: a spatiotemporal soliton is formed, which is characterized by the fact that its constituent modes remain mutually trapped in time. Remarkably, Fig. 1 reveals that, as a result of nonlinear coupling between the fundamental mode and the other two higher-order axial modes, after approximately 120 m of propagation virtually all of the input energy is funneled into the pulse carried by the fundamental mode, whereas higher-order modes decay into dispersive waves with negligible power, with a center wavelength close to the input value. The energy increase of the fundamental mode at the expense of higher-order modes can be approximated by an exponential law, specifically, $E_1(z) = E_{\text{in}}[1 - (1 - f_1)e^{(-s_1 z)}]$, with E_{in} the input energy, $f_1 = 0.52$ the initial power fraction of the fundamental mode, and s_1 a decay rate factor which depends on input pulse energy. Figure 1 shows that, in the subsequent 880 m of propagation, a substantially monomodal soliton propagates, experiencing progressive wavelength redshift caused by Raman SSFS. As

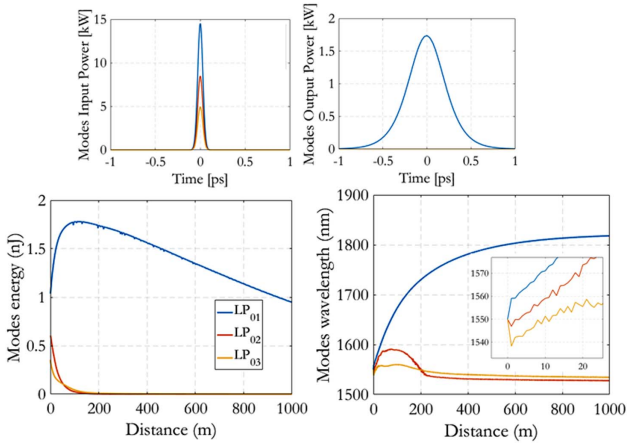

Fig. 1. Simulated energy and wavelength evolution of the three input axial modes. The two upper insets show the pulse power modal distribution at the input (left), and after 1 km of propagation (right).

the soliton wavelength increases above 1700 nm, it starts losing energy because of linear fiber attenuation: as a result, it broadens temporally, in order to adiabatically conserve the monomodal solitonic condition (top right inset). Additional numerical simulations performed with a larger number of input modes (not shown), obtained by injecting the input beam off-axis, confirm a similar behavior: a net energy transfer from all modes to the fundamental mode is always observed, but at a higher input power with respect to the case of axial injection.

In our coupled-mode simulations, we did not include the presence of random linear mode coupling. In Ref. [33], the role of random mode coupling was investigated in MDM transmission systems; it was shown that the correlation length L_{cm}, characterizing random mode coupling, is of the order of tens of meters for degenerate modes, and hundreds of meters for nondegenerate modes. In Ref. [34] it was shown that, both in the case of weak mode coupling (i.e., a random mode coupling correlation length L_{cm} much longer than the correlation length of random polarization birefringence L_{cp}), and in the case of strong mode coupling (i.e., when L_{cm} is comparable with L_{cp}), pulse propagation may be described in terms of generalized Manakov equations. This is justified whenever one may assume that L_{cm} and L_{cp} are both smaller than the nonlinearity length, L_{NL}.

In Ref. [35] intermodal (IM)-FWM was analyzed in few-mode fibers, in the presence of both linear random mode coupling and random birefringence. In that work, the random birefringence correlation length L_{cp} was supposed to range between a meter and a few tens of meters. It was shown that the IM-FWM efficiency may be lowered by up to 40 dB if $L_{cm} \ll L_{NL}$; whereas in the absence of random mode coupling, the IM-FWM efficiency is maximized under the condition of phase matching, which generally involves the coupling of modes at different wavelengths. Moreover, in Ref. [8] it was shown analytically that, in the case of multimodal transmissions with $L_{cm} < L_{NL}$, nonlinear interactions between degenerate modes can be averaged, owing to strong linear coupling between modes within each group. Based on this assumption, a set of generalized Manakov equations was obtained, that admit for an exact solution in the form of a vector hyperbolic secant solitary wave.

In our work, numerical simulations reveal the presence of a more complex dynamics that occurs in a different, strongly nonlinear regime, i.e., whenever the nonlinearity length $L_{NL} = \lambda w_e^2/(2n_2P_p)$ (here w_e is the effective beam waist and P_p is the pulse peak power) is much shorter than the typical correlation lengths of random linear mode coupling and polarization birefringence. In other terms, in our case nonlinearity acts over scales that are much shorter than the typical length scale which can be described in terms of generalized Manakov equations, so that FWM-induced energy exchange between nondegenerate modes is not averaged out by linear modal coupling.

Spatiotemporal solitons, involving the nonlinear coupling of nondegenerate modes, are generated over distances in the range of a few nonlinearity lengths, provided that L_{NL} is comparable with the modal walk-off length. In the example of Fig. 1 and also in our experiments, after a few meters of distance a multimode soliton with the initial pulse width of 120 fs is generated. This corresponds to a nonlinearity length of 18 cm, which is equal to the chromatic dispersion length; the modal walk-off length is approximately 22 cm, which is also comparable to L_{NL}. Once the modes are temporally trapped, the spatiotemporal soliton experiences a Raman-induced wavelength redshift or SSFS.

As a result of SSFS, the pulse width of the fundamental soliton increases almost linearly with distance, because of the wavelength increase that leads to experiencing progressively larger (in absolute value) chromatic dispersions, and the consequent need to maintain the solitonic energy $E_1 = \lambda|\beta_2(\lambda)|w_e^2/(n_2T_0)$, with $T_0 = T_{FWHM}/1.763$. The increase with distance of the soliton pulse width can be approximated by the law $T_0(z) = T_0(z_f)[1 + s_2(z - z_f)]$, where s_2 is a slope which depends on input peak power, and z_f is the initial distance of soliton formation.

Simulations of Fig. 1 predict that a slow power transfer from higher-order modes into the fundamental mode occurs upon propagation. This process is completed at distance in the range of hundreds or even thousands of nonlinearity lengths. After 100–150 m of propagation, the resulting soliton is substantially monomodal. In Refs. [25,36], the phenomenon of spatial beam self-cleaning was introduced and described as a process of beam condensation, induced by the combination of the Kerr effect and spatial self-imaging in a GRIN fiber, that can be accelerated by the presence of random polarization coupling. In our work, the slow and irreversible energy transfer into the fundamental mode is only observed in the anomalous dispersion region of the fiber, at input powers leading to spatiotemporal Raman soliton formation. Therefore, we attribute the observed effect to non-phase-matched modal FWM and stimulated Raman scattering (SRS) processes, providing a net energy transfer into the fundamental mode under the condition for multimode soliton generation, i.e., when the propagating modes are mutually temporally trapped, and subject to Raman SSFS.

B. Experimental Evidence over 1 km of GRIN Fiber

In order to experimentally confirm the generation of monomodal solitons over long spans of GRIN multimodal fiber, a testbed was prepared by using femtosecond pulses propagating over 1 km of fiber. The experimental setup used for the generation of MMF solitons consists of an ultrashort laser system, including a hybrid optical parametric amplifier of white-light continuum (Lightconversion ORPHEUS-F), pumped by a femtosecond Yb-based laser (Lightconversion PHAROS-SP-HP), generating pulses at 100 kHz repetition rate with Gaussian beam shape ($M^2 = 1.3$); the pulse temporal shape at 1550 nm is nearly Gaussian, with 67 fs pulse width. The laser beam is focused by a 50 mm lens into the fiber with $1/e^2$ input diameter of approximately 30 μm. Laser pulses enter the fiber with peak powers ranging between 100 W and 500 kW, which is regulated by using an external attenuator. The used fiber is a 1 km span of commercial parabolic GRIN fiber, with core radius $r_c = 25$ μm, cladding radius 62.5 μm, cladding index $n_{clad} = 1.444$ at 1550 nm, and relative index difference $\Delta = 0.0103$. At the GRIN fiber output, a micro-lens focuses the near field on an InGaAs camera (Hamamatsu C12741-03); a second lens focuses the beam into

an optical spectrum analyzer (Yokogawa AQ6370D) with a wavelength range of 600–1700 nm, and into a real-time multiple octave spectrum analyzer (Fastlite Mozza), with a range of 1100–3000 nm. The output pulse temporal shape is inspected by using an infrared fast photodiode and an 8 GHz digital oscilloscope with 30 ps overall time response (Teledyne Lecroy WavePro 804HD), and an intensity autocorrelator (APE pulseCheck 50) with femtosecond resolution.

Figure 2 shows an example of measured spectra (left column), photodiode traces (central column), and output near fields (right column) after 1 km of fiber transmission, for input pulse peak powers of 2 kW, 6.4 kW, 15 kW, and 110 kW, respectively. At input peak power levels corresponding to the linear propagation regime (e.g., 2 kW), the output spectrum [see Fig. 2(a)] is nearly identical to that of the input pulse, whereas the output pulse has temporally broadened to 1.2 ns, as a consequence of cumulated chromatic and modal dispersion. At 6.4 kW of peak power, an intermediate regime is observed, where self-phase modulation (SPM) nonlinearity starts counteracting dispersion, but it is not able to form a soliton yet: in the first few meters of propagation, the cumulated anomalous dispersion interacts with SPM, producing a rapid bandwidth compression and distortion of the chirped pulse [see Fig. 2(b)] [37]. At 15 kW of peak power, a spatiotemporal soliton starts to be formed [see Fig. 2(c)], and it experiences a Raman-induced SSFS [38]. As it can be seen, the recorded pulse is temporally narrower, and it is delayed with respect to the residual dispersive wave. In the soliton regime, the pulse bandwidth $\Delta\nu$ is not as narrow as in the intermediate regime; instead, it depends on the soliton pulse width as $\Delta\nu = 0.315/T_{\mathrm{FWHM}}$. For input peak powers above 50 kW, the input pulse undergoes soliton fission, generating multiple spatiotemporal solitons with comparable pulse width [17]. The first soliton is the more energetic, and therefore it suffers a larger SSFS with respect to the others. Figure 2(d) shows two spectra formed from an input pulse with 110 kW peak power; the photodiode trace gives evidence of two propagating pulses, the right one being affected by a Raman-induced relative delay. A third soliton is also observed at higher powers. Each of the generated solitons shows a behavior similar to that of the first Raman soliton.

The temporal evolution of the different solitons generated at the fiber output is better illustrated by the animation in Visualization 1, where the traces from the fast photodiode have been represented for increasing values of the input peak power.

With the help of numerical simulations, we predicted the formation of monomodal solitons after 100–150 m of propagation in a GRIN fiber. The experimental results demonstrate that more complex multimode soliton dynamics takes place when the input power grows substantially larger than the threshold for single soliton formation. Specifically, a train of monomodal solitons is generated across a wide range of input powers.

As it is illustrated in Fig. 2, recorded soliton spectra at 1 km distance are characterized by lobes with a sech shape: we measured their peak wavelength and bandwidth. The plots in Fig. 3 (top) report the evolution of the output spectra versus input peak power, and show that, for input powers between 10 kW and 43 kW, a first soliton is generated that experiences Raman SSFS. Whenever the wavelength of this soliton exceeds 1950 nm, it is absorbed by the fiber because of linear fiber loss. Numerical simulations (blue empty circles) report data which are in good agreement with the experiments. Small discrepancies for wavelengths longer than 1900 nm can be attributed to an over-estimation of the silica attenuation with respect to real fiber losses. For input peak powers between 60 kW and 190 kW, a second soliton is measured with a similar spectral shift, until a third soliton appears for input powers above 130 kW. The three solitons coexist in the fiber, but the first and second solitons are progressively absorbed when their

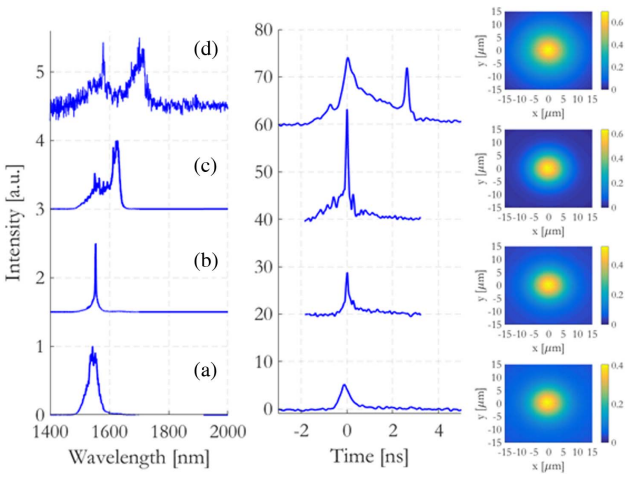

Fig. 2. Measured output spectra (left column), photodiode traces (center column), and near-field (right column) at 1 km distance, for input pulse peak powers of (a) 2 kW, (b) 6.4 kW, (c) 15 kW, and (d) 110 kW (see Visualization 1).

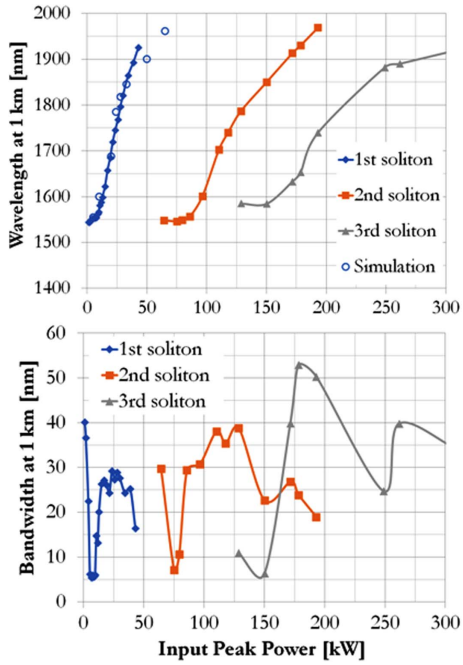

Fig. 3. Top: Measured wavelength for the three generated solitons versus input peak power. Bottom: corresponding soliton bandwidth evolution.

wavelengths reach the 1900–2000 nm wavelength region. From Fig. 3 (bottom), it can be confirmed that a strong reduction of the pulse bandwidth occurs at input peak powers immediately below the value for soliton formation, as already discussed above.

As the soliton propagates through the parabolic GRIN fiber, its multimodal beam waist undergoes fast self-imaging oscillations [39,40]. In this regime, the ratio of minimum to maximum beam effective area can be provided by the variational approach theory as [20,23] $C = \lambda^2 r_c^2/(2\pi^2 \Delta n_{\text{eff}}^2 w_e^4)$, with $r_c = 25$ μm the core radius, $\Delta = 0.0103$ the relative core–cladding index difference, and $n_{\text{eff}} = 1.459$ the effective core index for the propagating mode. The effective beam waist w_e is calculated for the fundamental mode by setting $C = 1$; therefore, $w_{e1} = (\lambda^2 r_c^2/2\pi^2 \Delta n_{\text{eff}}^2)^{1/4}$, and equals $w_{e1} = 7.7$ μm in our case.

Figure 4 shows the measured output beam waist after 1 km of propagation, for increasing values of the input peak power; the beam size is compared with the theoretical monomodal value (horizontal dashed line). In order to enhance the beam cleaning effect, we coupled the input beam with different tilt angles, i.e., of 0°, 2.3°, and 4.6°, respectively.

At a peak power of 15 kW and tilt 0°, when the MMF solitonic pulse is formed and it starts experiencing Raman SSFS, the beam recorded at 1 km distance shows a strong diameter reduction down to the value of 8.5 μm, behaving as a substantially self-cleaned, monomodal soliton, as predicted by numerical simulations. We measured in this condition the beam M^2, with a calibrated and automated optical system (Gentec Beamage M^2), obtaining a value of 1.45. For higher powers, the beam recovers a large waist. However, Fig. 4 shows that the second and the third solitons also experience a beam width reduction (at 110 kW and at 190 kW, respectively), although their spatial compression is limited by the presence of multiple pulses and dispersive waves.

At an input tilt angle of 2.3°, we calculated that the power distribution between the modes at the input is 12%, 12%, 12%, 8.6%, and 5.3% for modes LP_{01}, LP_{11e}, LP_{11o}, LP_{21}, and LP_{02}, respectively, and it also contains smaller proportions of higher-order modes. At 4.6° input angle, the power distribution is even more uniform. As a consequence, the generation of a fundamental soliton could still be measured at the fiber output, but for input powers that were increased by a factor of 5 with respect to the case of pure axial incidence. Still, a fundamental soliton was observed at 70–80 kW of input peak power, with the output beam waist of 8.8 μm, close to the value of the fundamental mode. It is interesting to note that the second and third solitons are still capable to produce virtually monomodal solitons with 2.3° input angle, demonstrating that the attraction property into the fundamental mode is not exclusive of the lowest-power soliton.

The insets in Fig. 4 show the recorded output near fields when the input tilt angle is 2.3°: the formation of a narrow, cleaned beam at the input power of 72 kW can be clearly seen, corresponding to the generation of a spatiotemporal fundamental mode soliton (central inset). This can be compared to the multimodal output beam which is obtained at low powers (16 kW, left inset); whereas at higher input energies, the breakup of the soliton and the generation of dispersive waves produce wider beams, and in some cases higher-order mode patterns (230 kW, right inset). At the soliton power, we measured a beam quality factor $M^2 = 1.4$, which is close to the value $M^2 = 1.3$ of the input laser beam.

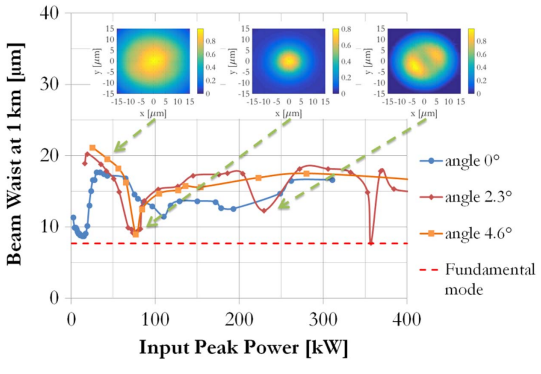

Fig. 4. Measured beam waist at 1 km distance versus input peak power, when the input beam is coupled with 0°, 2.3°, and 4.6° tilt angle, as compared with the theoretical fundamental mode waist. Input beam waist is 15 μm. Insets show measured output beam shapes at powers indicated by the arrows.

C. Experimental Results over 120 m of GRIN Fiber

Numerical simulations in Section 2.A have shown that, at a distance of approximately 120 m and at the solitonic power, nearly all of the pulse energy is nonlinearly transferred into the fundamental mode of the GRIN MMF (see Fig. 1). For longer distances, the wavelength shifted pulse starts suffering the effects of linear fiber loss. This observation led us to perform a soliton transmission experiment using a 120 m span of GRIN fiber, in order to observe and characterize the newly generated monomodal spatiotemporal soliton in the temporal, spatial, and frequency domains, respectively.

Figure 5 shows the output pulse width of the soliton as it was measured by autocorrelations: experimental results are compared to simulations at 120 m. The top insets show auto-

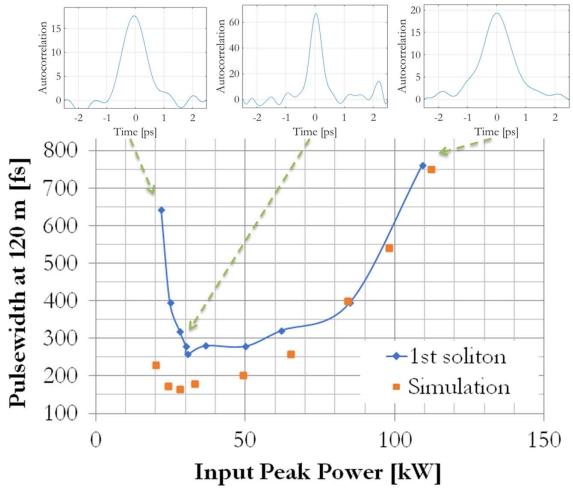

Fig. 5. Measured and simulated FWHM pulse width at 120 m distance versus input peak power. The top insets are autocorrelation traces at 21 kW, 28 kW, and 109 kW input power, respectively.

correlation traces at 21 kW, 28 kW, and 109 kW input power, respectively. A minimum pulse width soliton was measured at the input peak power of 25–30 kW, with a temporal duration of $T_{\mathrm{FWHM}} = 260$ fs, against the simulated duration of 180 fs: the discrepancy may be attributed to dispersive effects from the output optics. Experiments and simulations performed with 10 m of fiber (not shown) provided output spatiotemporal solitons with 120 fs pulse width, and dispersion/nonlinearity length of 18 cm. The pulse width increases with distance or for higher input powers, because of the soliton wavelength increase induced by SSFS, so that it experiences a larger amount of anomalous chromatic dispersion. As a result, the pulse duration must grow larger in order to keep the fundamental soliton condition unchanged.

Figure 6 shows the measured bandwidth of the spectral lobes corresponding to the first and second solitons, at 120 m distance; we also included the corresponding simulation results for the first soliton. At 15–20 kW of input peak power, the output pulse experiences a bandwidth compression down to 14 nm, before the phase of soliton formation. At 25–30 kW of input peak power, the first soliton has formed: the corresponding output bandwidth increases up to about 20 nm. Figure 6 also shows that the bandwidth of the second soliton, which is generated at input powers around 165 kW, exhibits a similar behavior.

As far as the measured beam waist at 120 m is concerned, Fig. 7 shows that, at 27–30 kW of input peak power, a minimum of output beam waist of 8.8 μm is reached, which again is close to the monomodal value of 7.7 μm. It is noteworthy that the curve of the output beam waist as a function of input peak power, in Fig. 7, is narrower with respect to that for the measured pulse width in Fig. 5. This can be explained with the help of the numerical results of Fig. 1: as can be seen, the soliton mostly carried by the fundamental mode suffers a wavelength shift in the first 120 m, up to 1700 nm and beyond, thus experiencing linear losses that grow larger with distance. For input energies right above the optimal soliton value, the total linear propagation losses suffered by the fundamental mode may become so high that its output energy becomes comparable to that of the residual higher-order modes, which remain at the minimum loss wavelength region around 1550 nm. As a result, at the fiber output the beam appears multimodal, as soon as the input pulse peak power grows right above the optimal soliton value.

In Fig. 8, the recorded autocorrelation traces are given alongside with the corresponding near-field of the beam, for

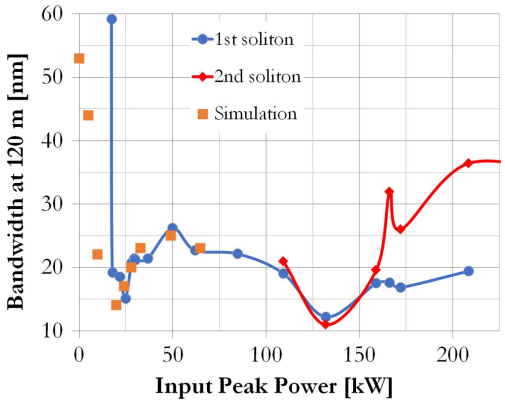

Fig. 6. Measured bandwidth versus input peak power, for the two solitons observed after 120 m of GRIN fiber.

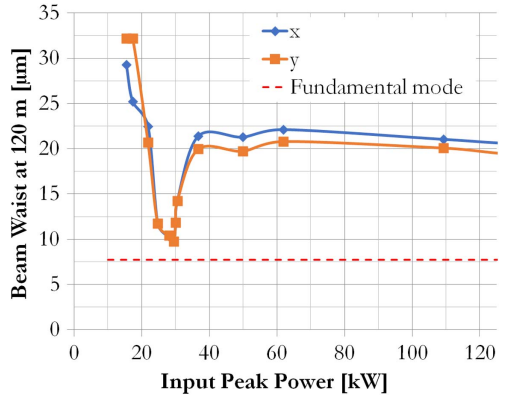

Fig. 7. Near-field beam waist versus input peak power, for the first soliton at 120 m of GRIN fiber length.

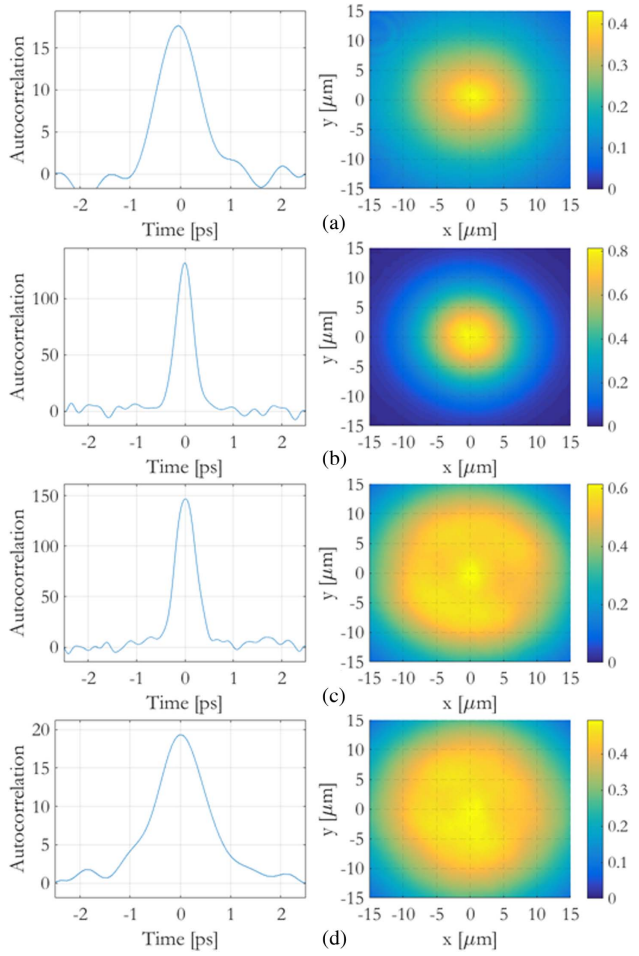

Fig. 8. Recorded autocorrelation traces (left column) and near-field beams (right column) from 120 m of GRIN fiber, for input peak powers: (a) 22 kW, (b) 29 kW, (c) 37 kW, and (d) 109 kW.

the input peak powers: 22 kW, 29 kW, 37 kW, and 109 kW, respectively. As it can be seen, in the stage preceding soliton formation, at 22 kW of input peak power, the output beam is still relatively wide, while the pulse bandwidth reaches its minimum value (see Fig. 6). At the power of 29 kW, a spatiotemporal fundamental soliton is generated: pulse duration and beam waist simultaneously reach their minima, i.e., 260 fs and 8.8 μm, respectively, whereas the pulse bandwidth starts to increase. At 37 kW of input peak power, the output pulse width is still limited to 280 fs. To the contrary, the beam is no longer confined to a single mode, and the waist has more than the doubled with respect to the fundamental soliton case; still, we may talk of a multimodal, spatiotemporal soliton in this case. For higher powers (109 kW) the pulse starts broadening in time, and the multimodal soliton condition is gradually lost.

Finally, from the simulated and measured data we can calculate the soliton order at both 120 m and 1 km of GRIN fiber length, by using the formula $N = \{n_2 T_0 E_1/[\lambda|\beta_2(\lambda)|w_e^2]\}^{1/2}$. By using the fiber dispersion value at the soliton wavelength, the simulated output energy and pulse width, and the effective waist $w_{e1} = 7.7$ μm obtained from the variational theory, we obtain that, for a solitonic input peak power of 28 kW, the order is $N = 1.17$ at 120 m and $N = 1.03$ at 1 km. Those results indicate that, in spite of the linear losses, a fundamental soliton of order 1 was reached at 1 km distance. At 120 m the effective waist to be used in the formula to obtain $N = 1$ is $w_e = 8.8$ μm, which is exactly the value of the measured beam waist (see Fig. 7).

3. CONCLUSION

Spatiotemporal soliton evolution in parabolic GRIN fibers was previously described, by using the variational approach, as a stable propagation of a self-imaging beam; in this picture, the several modes formed at the input trap each other and indefinitely preserve their temporal shape. In this work we demonstrated, both experimentally and numerically, that the spatiotemporal soliton evolution over long spans of fiber is far more complex: a pump pulse feeds a spatiotemporal soliton at proper input energy when the nonlinearity length of the forming soliton is comparable to the modal walk-off length. The modes effectively trap each other in time but, in the range of hundreds of nonlinearity lengths, a slow and irreversible energy transfer is observed from higher-order modes into the fundamental mode of the fiber, which acts as a dynamical attractor of the multimode system. The spatiotemporal soliton thus naturally evolves into a single-mode soliton, and it permanently maintains this state. The optimal energy where the single-mode, minimum waist beam is observed at the fiber output corresponds to that of minimum output pulse width. The pulse bandwidth suffers a bandwidth reduction previous to the optimal solitonic power and increases to the solitonic value at optimal energy. The output soliton order results are unitary if the effective beam waist is considered equal to the single-mode value.

To place our findings in a broader perspective, we anticipate that our results will be of general fundamental interest, because they provide the first example of fully spatiotemporal beam condensation in classical nonlinear wave systems [41]. From the point of view of technological applications, the generation of a robust ultrashort soliton attractor in a nonlinear multimode fiber is of significance for the delivery of high-energy laser beams in a variety of industrial applications, for high-power spatiotemporal mode-locked multimode fiber lasers [42], and for the use of multimode fibers in high-bit-rate fiber optic networks.

Funding. European Research Council (740355 (STEMS), 874596); Ministero dell'Istruzione, dell'Università e della Ricerca (R18SPB8227); Ministry of Education and Science of the Russian Federation (14.Y26.31.0017).

Acknowledgment. We thank Wright *et al.* for making freely available the open-source parallel numerical mode solver for the coupled-mode nonlinear Schrödinger equations [30], and Oleg Sidelnikov for developing a mode decomposition numerical code. We acknowledge the financial support from the European Research Council Advanced, the Italian Ministry of University and Research, and the Russian Ministry of Science and Education.

Disclosures. The authors declare no conflicts of interest.

REFERENCES

1. A. Hasegawa and M. Matsumoto, *Optical Solitons in Fibers* (Springer, 2003).
2. V. E. Zakharov and S. Wabnitz, *Optical Solitons: Theoretical Challenges and Industrial Perspectives* (Springer, 1999).
3. A. Hasegawa, "Self-confinement of multimode optical pulse in a glass fiber," Opt. Lett. **5**, 416–417 (1980).
4. B. Crosignani and P. D. Porto, "Soliton propagation in multimode optical fibers," Opt. Lett. **6**, 329–330 (1981).
5. B. Crosignani, A. Cutolo, and P. D. Porto, "Coupled-mode theory of nonlinear propagation in multimode and single-mode fibers: envelope solitons and self-confinement," J. Opt. Soc. Am. **72**, 1136–1141 (1982).
6. K. Krupa, A. Tonello, A. Barthélémy, T. Mansuryan, V. Couderc, G. Millot, P. Grelu, D. Modotto, S. A. Babin, and S. Wabnitz, "Multimode nonlinear fiber optics, a spatiotemporal avenue," APL Photonics **4**, 110901 (2019).
7. D. J. Richardson, J. M. Fini, and L. Nelson, "Space-division multiplexing in optical fibres," Nat. Photonics **7**, 354–362 (2013).
8. A. Mecozzi, C. Antonelli, and M. Shtaif, "Coupled Manakov equations in multimode fibers with strongly coupled groups of modes," Opt. Express **20**, 23436–23441 (2012).
9. A. Mecozzi, C. Antonelli, and M. Shtaif, "Soliton trapping in multimode fibers with random mode coupling," arXiv:1207.6506 (2012).
10. G. Agrawal, *Fiber-Optic Communication Systems* (Wiley, 1997).
11. M. E. Fermann, "Single-mode excitation of multimode fibers with ultrashort pulses," Opt. Lett. **23**, 52–54 (1998).
12. N. O. Moussa, T. Mansuryan, C. H. Hage, M. Fabert, K. Krupa, A. Tonello, M. Ferraro, L. Leggio, M. Zitelli, F. Mangini, A. Niang, G. Millot, M. Papi, S. Wabnitz, and V. Couderc, "Spatiotemporal beam self-cleaning for high-resolution nonlinear fluorescence imaging with multimode fibres," arXiv:2010.09340 (2020).
13. W. H. Renninger and F. W. Wise, "Optical solitons in graded-index multimode fibres," Nat. Commun. **4**, 1719 (2013).
14. L. G. Wright, W. H. Renninger, D. N. Christodoulides, and F. W. Wise, "Spatiotemporal dynamics of multimode optical solitons," Opt. Express **23**, 3492–3506 (2015).
15. Z. Zhu, L. G. Wright, D. N. Christodoulides, and F. W. Wise, "Observation of multimode solitons in few-mode fiber," Opt. Lett. **41**, 4819–4822 (2016).

16. A. Antikainen, L. Rishøj, B. Tai, S. Ramachandran, and G. Agrawal, "Fate of a soliton in a high order spatial mode of a multimode fiber," Phys. Rev. Lett. **122**, 023901 (2019).
17. M. Zitelli, F. Mangini, M. Ferraro, A. Niang, D. Kharenko, and S. Wabnitz, "High-energy soliton fission dynamics in multimode grin fiber," Opt. Express **28**, 20473–20488 (2020).
18. S.-S. Yu, C.-H. Chien, Y. Lai, and J. Wang, "Spatio-temporal solitary pulses in graded-index materials with Kerr nonlinearity," Opt. Commun. **119**, 167–170 (1995).
19. S. Raghavan and G. P. Agrawal, "Spatiotemporal solitons in inhomogeneous nonlinear media," Opt. Commun. **180**, 377–382 (2000).
20. M. Karlsson, D. Anderson, and M. Desaix, "Dynamics of self-focusing and self-phase modulation in a parabolic index optical fiber," Opt. Lett. **17**, 22–24 (1992).
21. M. Conforti, C. M. Arabi, A. Mussot, and A. Kudlinski, "Fast and accurate modeling of nonlinear pulse propagation in graded-index multimode fibers," Opt. Lett. **42**, 4004–4007 (2017).
22. A. S. Ahsan and G. P. Agrawal, "Graded-index solitons in multimode fibers," Opt. Lett. **43**, 3345–3348 (2018).
23. A. S. Ahsan and G. P. Agrawal, "Spatio-temporal enhancement of raman-induced frequency shifts in graded-index multimode fibers," Opt. Lett. **44**, 2637–2640 (2019).
24. A. B. Grudinin, E. Dianov, D. Korbkin, A. M. Prokhorov, and D. Khaidarov, "Nonlinear mode coupling in multimode optical fibers; excitation of femtosecond-range stimulated-Raman-scattering solitons," J. Exp. Theor. Phys. Lett. **47**, 356–359 (1988).
25. K. Krupa, A. Tonello, B. M. Shalaby, M. Fabert, A. Barthélémy, G. Millot, S. Wabnitz, and V. Couderc, "Spatial beam self-cleaning in multimode fibres," Nat. Photonics **11**, 237–241 (2017).
26. Z. Liu, L. G. Wright, D. N. Christodoulides, and F. W. Wise, "Kerr self-cleaning of femtosecond-pulsed beams in graded-index multimode fiber," Opt. Lett. **41**, 3675–3678 (2016).
27. L. G. Wright, Z. Liu, D. A. Nolan, M.-J. Li, D. N. Christodoulides, and F. W. Wise, "Self-organized instability in graded-index multimode fibres," Nat. Photonics **10**, 771–776 (2016).
28. Y. Leventoux, A. Parriaux, O. Sidelnikov, G. Granger, M. Jossent, L. Lavoute, D. Gaponov, M. Fabert, A. Tonello, K. Krupa, A. Desfarges-Berthelemot, V. Kermene, G. Millot, S. Février, S. Wabnitz, and V. Couderc, "Highly efficient few-mode spatial beam self-cleaning at 1.5 μm," Opt. Express **28**, 14333–14344 (2020).
29. F. Poletti and P. Horak, "Description of ultrashort pulse propagation in multimode optical fibers," J. Opt. Soc. Am. B **25**, 1645–1654 (2008).
30. L. G. Wright, Z. M. Ziegler, P. M. Lushnikov, Z. Zhu, M. A. Eftekhar, D. N. Christodoulides, and F. W. Wise, "Multimode nonlinear fiber optics: massively parallel numerical solver, tutorial, and outlook," IEEE J. Sel. Top. Quantum Electron. **24**, 5100516 (2018).
31. R. H. Stolen, J. P. Gordon, W. J. Tomlinson, and H. A. Haus, "Raman response function of silica-core fibers," J. Opt. Soc. Am. B **6**, 1159–1166 (1989).
32. G. P. Agrawal, *Nonlinear Fiber Optics*, 3rd ed. (Academic, 2001).
33. K. Ho and J. Kahn, "Linear propagation effects in mode-division multiplexing systems," J. Lightwave Technol. **32**, 614–628 (2014).
34. S. Mumtaz, R.-J. Essiambre, and G. P. Agrawal, "Nonlinear propagation in multimode and multicore fibers: generalization of the Manakov equations," J. Lightwave Technol. **31**, 398–406 (2012).
35. Y. Xiao, R.-J. Essiambre, M. Desgroseilliers, A. M. Tulino, R. Ryf, S. Mumtaz, and G. P. Agrawal, "Theory of intermodal four-wave mixing with random linear mode coupling in few-mode fibers," Opt. Express **22**, 32039–32059 (2014).
36. A. Fusaro, J. Garnier, K. Krupa, G. Millot, and A. Picozzi, "Dramatic acceleration of wave condensation mediated by disorder in multimode fibers," Phys. Rev. Lett. **122**, 123902 (2019).
37. M. Zitelli, M. Ferraro, F. Mangini, and S. Wabnitz, "Managing self-phase modulation in pseudo-linear multimodal and monomodal systems," J. Lightwave Technol. **39**, 1953–1960 (2021).
38. F. M. Mitschke and L. F. Mollenauer, "Discovery of the soliton self-frequency shift," Opt. Lett. **11**, 659–661 (1986).
39. T. Hansson, A. Tonello, T. Mansuryan, F. Mangini, M. Zitelli, M. Ferraro, A. Niang, R. Crescenzi, S. Wabnitz, and V. Couderc, "Nonlinear beam self-imaging and self-focusing dynamics in a GRIN multimode optical fiber: theory and experiments," Opt. Express **28**, 24005–24021 (2020).
40. F. Mangini, M. Ferraro, M. Zitelli, A. Niang, A. Tonello, V. Couderc, and S. Wabnitz, "Multiphoton-absorption-excited up-conversion luminescence in optical fibers," Phys. Rev. Appl. **14**, 054063 (2020).
41. P. Aschieri, J. Garnier, C. Michel, V. Doya, and A. Picozzi, "Condensation and thermalization of classical optical waves in a waveguide," Phys. Rev. A **83**, 033838 (2011).
42. L. G. Wright, D. N. Christodoulides, and F. W. Wise, "Spatiotemporal mode-locking in multimode fiber lasers," Science **358**, 94–97 (2017).